Journal of Dental Sciences 19 (2024) 411–418

Available online at www.sciencedirect.com

ScienceDirect

journal homepage: www.e-jds.com

Original Article

Classification of the implant-ridge relationship utilizing the MobileNet architecture

Hao-Chieh Chang [a], Li-Wen Yu [a,b], Bo-Yi Liu [c], Po-Chun Chang [a,b,d*]

[a] *Graduate Institute of Clinical Dentistry, School of Dentistry, College of Medicine, National Taiwan University, Taipei, Taiwan*
[b] *Division of Periodontics, Department of Dentistry, National Taiwan University Hospital, Taipei, Taiwan*
[c] *Department of Biomechatronics Engineering, National Taiwan University, Taipei, Taiwan*
[d] *School of Dentistry, College of Dental Medicine, Kaohsiung Medical University, Kaohsiung, Taiwan*

Received 30 June 2023; Final revision received 1 August 2023
Available online 17 August 2023

KEYWORDS
Artificial intelligence;
Dental implants;
Alveolar process;
Implantology

Abstract *Background/purpose:* Proper implant-ridge classification is crucial for developing a dental implant treatment plan. This study aimed to verify the ability of MobileNet, an advanced deep learning model characterized by a lightweight architecture that allows for efficient model deployment on resource-constrained devices, to identify the implant-ridge relationship.
Materials and methods: A total of 630 cone-beam computerized tomography (CBCT) slices from 412 patients were collected and manually classified according to Terheyden's definition, preprocessed, and fed to MobileNet for training under the conditions of limited datasets (219 slices, condition A) and full datasets (630 cases) without and with automatic gap filling (conditions B and C).
Results: The overall model accuracy was 84.00% in condition A and 95.28% in conditions B and C. In condition C, the accuracy rates ranged from 94.00 to 99.21%, with F1 scores of 89.36–100.00%, and errors due to unidentifiable bone-implant contact and miscellaneous reasons were eliminated.
Conclusion: The MobileNet architecture was able to identify the implant-ridge classification on CBCT slices and can assist clinicians in establishing a reliable preoperative diagnosis and

* Corresponding author. Graduate Institute of Clinical Dentistry, School of Dentistry, College of Medicine, National Taiwan University, 1 Chang-Te St, Taipei 100, Taiwan.
E-mail address: changpc@ntu.edu.tw (P.-C. Chang).

https://doi.org/10.1016/j.jds.2023.08.002

treatment plan for dental implants. These results also suggest that artificial intelligence-assisted implant-ridge classification can be performed in the setting of general dental practice.

Introduction

Classification of the implant-ridge relationship is crucial in dental implant treatment planning. Understanding the pattern of bone loss allows clinicians to better prepare for the surgical procedure by allowing them to decide whether bone grafting is required before implant placement, to determine the optimal positioning of the implant, and to predict the prognosis of the implant.

Several classification systems have been developed to reflect the pattern and severity of alveolar bone loss. The Cawood and Howell classification categorizes the changes in alveolar bone shape following tooth extraction over time.[1] On the other hand, Seibert's classification classifies these changes based on the extent of vertical and horizontal alveolar bone defects.[2] The HVC ridge deficiency classification provides a more detailed classification by assessing the amount of horizontal and vertical bone loss separately.[3] Terheyden's classification, a more recently developed system, focuses on categorizing the defects in the alveolar bone that correspond to the position of the dental implant.[4]

However, the diagnostic process relies on the subjective interpretation of radiographic images by dental professionals, which requires extra-training and is potentially prone to bias and inconsistencies. Artificial intelligence (AI) has made significant advancements in recent years and has revolutionized various aspects of the medical field,[5] by leveraging AI algorithms, such as deep learning and computer vision. It has thus become possible to create a more objective, precise, and efficient classification system to assess the implant-ridge relationship.

Obtaining and annotating a large amount of data has always been a major challenge in AI-based training for medical images. The solutions include the reduction of features when the data source is limited and the development of automatic or semi-automatic annotation systems. Dataset preprocessing might be helpful for improving the accuracy of AI models on medical image identifications.[6,7] Convolutional neural network (CNN) architecture is a deep learning model that is specifically designed for processing grid-like structured data, such as images, and it utilizes convolutional layers, pooling layers, and fully connected layers to efficiently capture local features and perform feature extraction and classification.[8,9] Extensive CNNs, such as ResNet and U-Net, provide increased accuracy and performance in complex tasks.[10] However, they are associated with increased computational requirements, a larger memory footprint, and an increased processing time. These networks may not be suitable for the resource-limited environments, potentially impeding their practicality for dental applications.

MobileNet, an advanced CNN model, has emerged as a popular choice for medical diagnostic tasks such as skin disease classification,[11,12] and assessment of lung diseases with chest radiography.[6,13] In the traditional CNNs, a standard convolutional layer performs both filtering (extracting features) and combining (mixing features) in a single step. This approach can be computationally expensive, especially for deeper networks with a large number of parameters. The major characteristic of MobileNet is the use of depthwise separable convolutions, which filter the input channels independently and combine the output across channels, leading to significant reductions of computational demands and overall model size compared to the standard convolutions.[14] The lightweight architecture of MobileNet allows for efficient model deployment on resource-constrained devices, such as smartphones and embedded systems. This advantage is particularly useful in dental practices where high-performance computational resources might not be available. Through appropriate image preprocessing, MobileNet has demonstrated nearly equivalent performance to conventional CNNs.[15]

The aim of this study was to verify the ability of MobileNet architecture for identifying the relationship between the implant and alveolar bone on the cross-sectional image slices from cone-beam computed tomography (CBCT), and the contribution of data preprocessing in this architecture was also assessed. This model enabled the development of an AI-based automatic alveolar bone defect diagnostic evaluation system, which will assist clinicians to establish a reliable preoperative diagnosis and treatment plan, specifically the optimal timing for dental implant placement, the necessity for bone regeneration procedures, and whether a staged surgical approach should be considered. This advancement could also reduce decision inconsistencies among clinicians and prevent potential medical errors.

Materials and methods

Ethical approval and image selection

The Institutional Review Board of National Taiwan University Hospital (NTU) granted approval for this study (No.202209110RIND), and the study adhered to the 1975 Declaration of Helsinki as revised in 2000.[16] Due to the retrospective and non-interventional design of the study

and anonymous data analysis, informed consent was not required. CBCT images from the Department of Dentistry's Radiographic Unit at NTUH captured between March and September 2016 using a CBCT scanner (3D Accuitomo XYZ Slice View Tomograph; Morita, Kyoto, Japan) and i-Dixel 3DX software (version 2.2.1.3) were included if they met the following specified criteria:

1. Patients aged ≥20 years;
2. Patients with one or multiple missing dentition in the posterior mandibular area, excluding the third molars;
3. Patients without any detectable pathological conditions such as bone tumors or cysts on CBCT;
4. Patients without prior bone augmentation or surgical procedures conducted in the edentulous area; and
5. Patients without a history of use of medications that could potentially influence bone metabolism.

Virtual implant placement

Utilizing a computer-guided implant treatment software (Simplant Master 2011 V14.0.0.102, Materialise Dental n.v., Leuven, Belgium), the CBCT images were reconstructed. A proficient periodontist (LWY) virtually positioned the implant fixtures (10 mm length) in the edentulous sections of the CBCT images, following the following established criteria:

1. Ensuring an appropriate inter-occlusal distance and emergence profile, the top of the fixture was situated near the alveolar crest of the neighboring teeth.
2. To guarantee the maximum intercuspation and harmonized alignment for the future prosthesis, the center of the fixture in the buccolingual aspect was positioned in the occlusal table.
3. For premolars, the width of fixture was 4 mm, while for molars, it was 5 mm.

Ridge classification and labeling

Based on Terheyden's classification,[4] the mandibular edentulous ridges were categorized into the following five types according to their anatomical features:

Type 0/4: The buccal and lingual aspects of the implant are fully supported by alveolar bone.

Type 1/4: The buccal bone support is reduced by less than 50% of the implant length without obvious reduction of lingual bone support.

Type 2/4: The buccal bone support is reduced by 50% or more of the implant length without obvious reduction of lingual bone support.

Type 3/4: Both the buccal and lingual/palatal bone supports are obviously reduced, and the reduction of lingual bone support is less than 50% of the implant length.

Type 4/4: Both the buccal and lingual bone supports are reduced by 50% or more of the implant length.

Two experienced periodontists (CHC and LWL) labeled the classifications of edentulous ridges based on the implant position observed in the slices.

Image preprocessing

The flow of image preprocessing is illustrated in Fig. 1. The original image was reoriented to upright and centralized along the long axis of the implant to isolate a rectangular region of interest (ROI), which was bound by the top and bottom of a centralized implant. The ROI was cropped, resized to 225x225 pixels, and converted to a grayscale image.

To minimize interference from the implant in the deep learning model, a mask was created to cover the implant area. The contrast of the images was adjusted using the convertScaleAbs function from OpenCV Library (adjusted, alpha = 1.7, beta = 0), followed by K-means clustering to divide the images into three threshold levels. The images were then normalized, and their grayscale values were transformed to 0, 127, and 255.

To fill the hollow areas within the ridge, the cv2.findContours function from OpenCV Library was employed. In cases in which the outer edges of the bone contour were discontinuous on the image, the region connecting the center of the implant masked in the horizontal direction was filled to maximally delineate the range of the alveolar bone.

CNN for deep learning

MobileNet was used to classify the implant-ridge relationship. This architecture utilizes depthwise separable convolutions that consist of two distinct layers: depthwise convolution and pointwise convolution. In the depthwise convolution layer, a single filter is applied to each input channel. The outputs of the depthwise convolution are then combined using a 1×1 pointwise convolution.

The images were stratified into three groups for model training and testing: training data, validation data, and test data, with a ratio of 7:1:2, and the MobilelNet models were trained for 50 epochs with the Adam optimizer and evaluated with the validation group. Nvidia Geforce RTX 2080ti GPU, Intel Core i9-9900K CPU, and the Tensorflow 2.0 toolkit were used for the network.

Data presentation and model performance

The datasets were run using three conditions: the limited image dataset (219 slices) without automatic gap filling (condition A), the full dataset (630 slices) without automatic gap filling (condition B), and the full dataset (630 slices) with automatic gap filling (condition C).

All data are presented as the mean ± standard deviation. A confusion matrix was used to evaluate the model performance, and the following parameters were assessed:

$$\text{Accuracy} = \frac{True\ positive\ (TP) + true\ negative}{Total\ examined\ datasets}$$

$$\text{Precision} = \frac{TP}{TP + false\ positive\ (FP)}$$

$$\text{Recall} = \frac{TP}{TP + false\ negative\ (FN)}$$

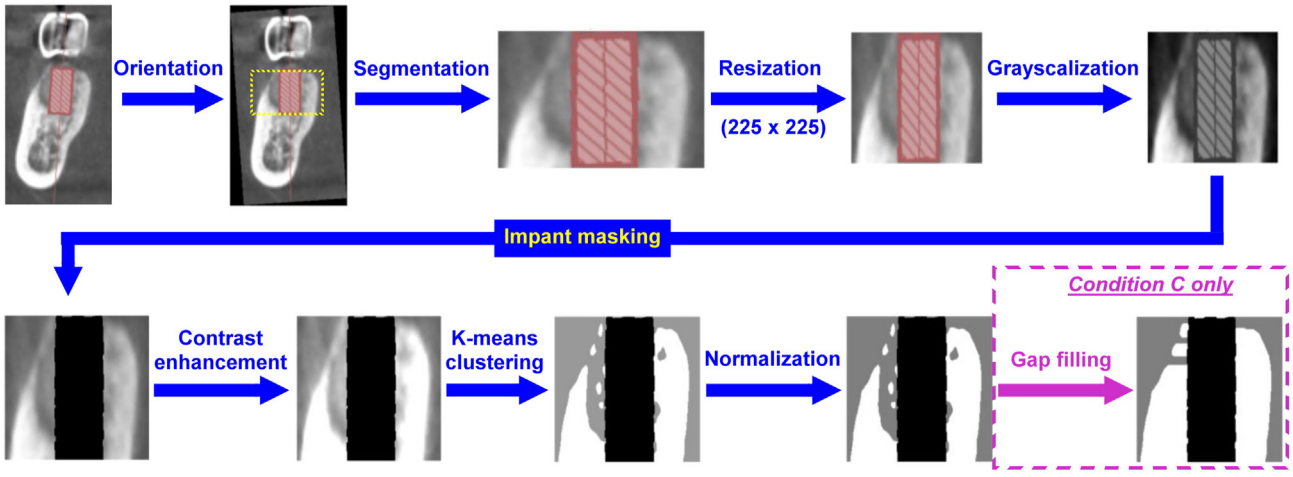

Figure 1 The image preprocessing process. Initially, the image slice was re-oriented according to the long axis of the dental implant, and ROI segmentation was performed. The image was then resized to a standardized dimension and converted to a grayscale-type image. Subsequently, the implant region is masked to reduce interference, and the contrast enhancement was performed. The K-means clustering method is used for block labeling after standardization. The image was then normalized and fed to MobileNet for training. In Condition C, an additional process called 'gap filling' was applied. This algorithm involved capturing the contour of the alveolar bone and filling the area horizontally towards the implant region.

$$\text{F1 score} = \frac{2 * TP}{2 * TP + FP + FN}$$

Results

A total of 630 image slices from 412 patients (198 males and 214 females aged 56.27 ± 12.34 years) were included in the datasets in this study. The distribution of each class and group is presented in Table 1.

Model performance

Among all the preprocessed images, the model accuracy was 84.00% in condition A, 95.28% in condition B, and 95.28% in condition C. The model performance according to the implant-ridge relationship is shown in Table 2.

Table 1 The distribution and the arrangement of datasets.

	Total sites	Training datasets	Validating datasets	Test datasets
Condition A	219	169	None	50
Type 0/4	55	45	None	10
Type 1/4	64	54	None	10
Type 2/4	32	22	None	10
Type 3/4	37	27	None	10
Type 4/4	31	21	None	10
Condition B/C	630	441	62	127
Type 0/4	162	112	16	34
Type 1/4	146	103	15	28
Type 2/4	104	74	10	20
Type 3/4	113	79	11	23
Type 4/4	105	74	10	21

The accuracy, precision, recall, and F1 score in condition A was lower than those in conditions B and C. The F1 score was generally >90% in conditions B and C, and the highest F1 score was noted in type 0/4 in condition C (100%), while type 3/4 in condition C had the lowest F1 score (89.36%). In conditions B and C, the precision was the lowest in type 2/4 in condition B (86.96%), and the recall was the lowest in type 3/4 of condition C (87.5%).

Prediction errors

In condition A, the images with prediction errors could be categorized into the following types: artifact disturbance, which included the superimposition of the opposite

Table 2 Model performance of the mandibular datasets based on the defect types.

Condition A	0/4	1/4	2/4	3/4	4/4
Accuracy (%)	98.00	94.00	88.00	90.00	94.00
Precision (%)	100.00	72.73	72.73	72.73	100.00
Recall (%)	91.67	100.00	72.73	80.00	70.00
F1 score (%)	95.65	84.21	72.73	76.19	82.35
Condition B	**0/4**	**1/4**	**2/4**	**3/4**	**4/4**
Accuracy (%)	98.43	98.43	97.64	98.43	97.63
Precision (%)	100.00	96.43	86.96	95.65	95.00
Recall (%)	94.12	96.43	100.00	95.65	90.48
F1 score (%)	96.97	96.43	93.02	95.65	92.68
Condition C	**0/4**	**1/4**	**2/4**	**3/4**	**4/4**
Accuracy (%)	100.00	96.85	99.21	96.06	98.43
Precision (%)	100.00	93.33	95.24	91.30	95.24
Recall (%)	100.00	93.33	100.00	87.50	95.24
F1 score (%)	100.00	93.33	97.56	89.36	95.24

occlusion or the surgical stent, a radiographic artifact associated with air, a discontinuous cortical bone plate, or other imaging characteristics that caused incorrect threshold determination (Fig. 2A); unidentifiable bone-implant contact caused by thin alveolar bone or a large bone marrow space adjacent to the implant (Fig. 2B); and miscellaneous errors, which referred to bone-implant contact that was identifiable and consistent with the original images after preprocessing but still resulted in incorrect model prediction. Miscellaneous errors were noted in most types of implant-ridge relationships except for types 0/4 and 1/4. (Fig. 2C).

In condition B, artifact disturbance (Fig. 3A) was still observed. Two images revealed unidentifiable bone-implant contact due to the misdetection of thin alveolar bone plates (Fig. 3B). One case of type 0/4 presented miscellaneous errors (Fig. 3C).

In condition C, six images demonstrated artifact disturbance (Fig. 4). None of the images showed unidentifiable bone-implant contact or miscellaneous errors.

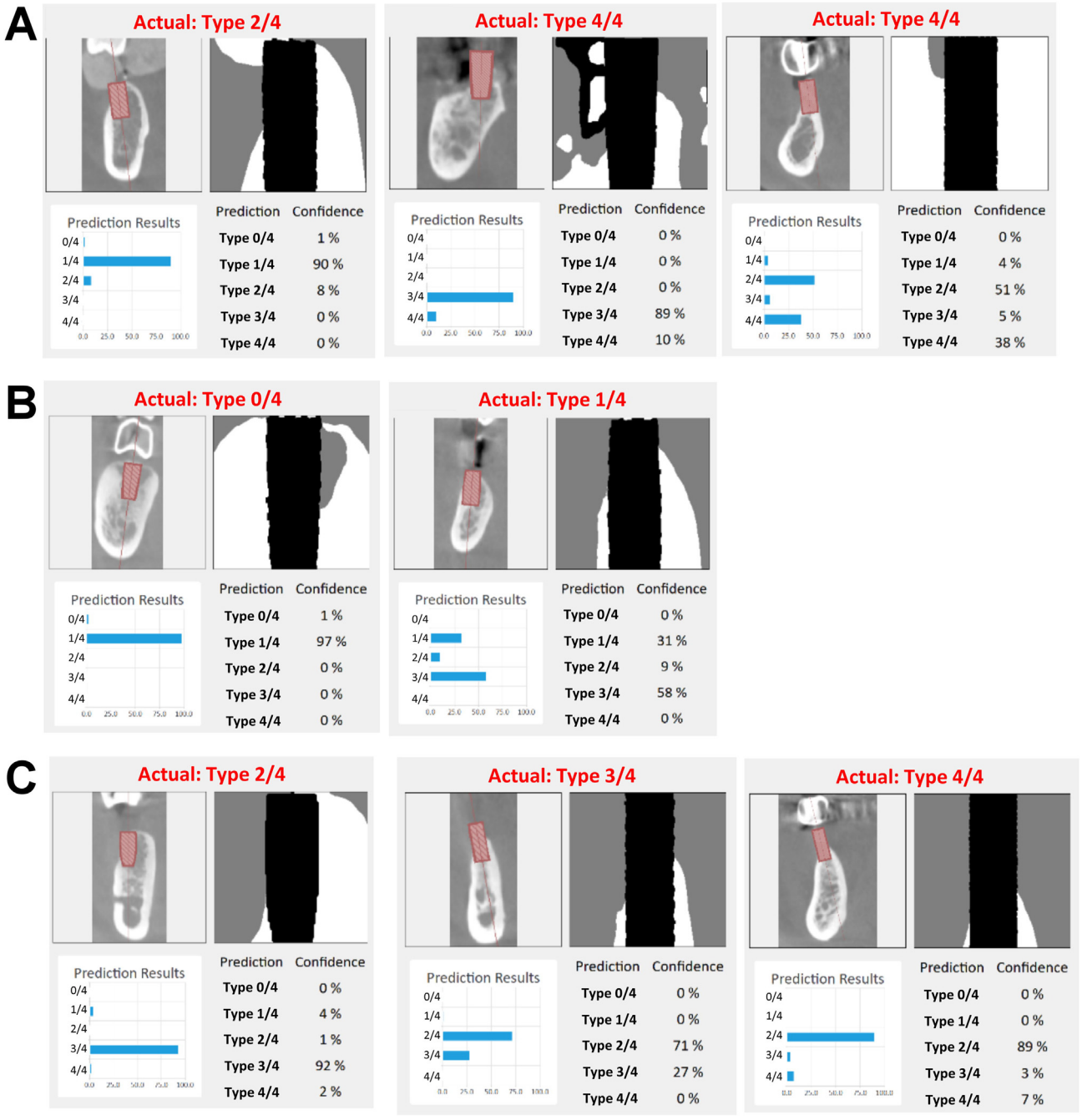

Figure 2 The cases of incorrect classification in condition A. (A) artifact disturbance. (B) Unidentifiable bone-implant contact. (C) miscellaneous errors.

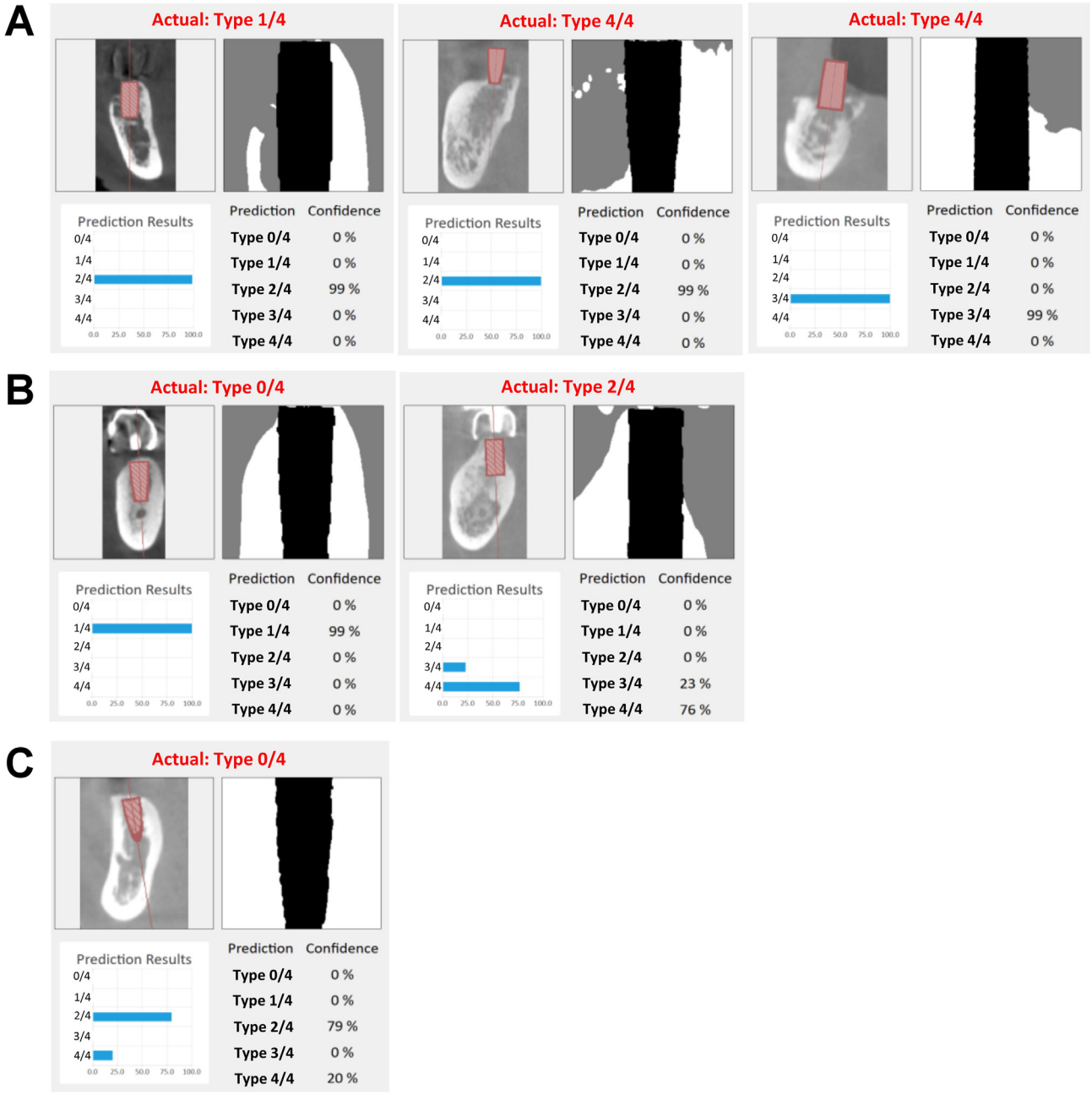

Figure 3 The cases of incorrect classification in condition B. (A) artifact disturbance. (B) Unidentifiable bone-implant contact. (C) miscellaneous errors.

Discussion

In this study, we established a CBCT database to identify the implant-ridge relationship from 630 sites in 420 patients. This database can be used to train AI models in related research fields. MobileNet, a deep learning model with a CNN architecture and reduced computational complexity that can be utilized efficiently on mobile devices or lightweight laptops,[17] was employed for data training and achieved accuracy rates of 94.00—99.21% and F1 scores of 89.36—100.00%. The outcome was comparable to the findings of our previous investigation using a ResNet-50 model, which is a conventional CNN architecture with greater computational complexity, that demonstrated an overall accuracy of 99.52—99.84% with an F1 score of 97.3—99.96%. The results from this study implied that this AI model can be used in situations with limited access to information technology and that it was capable of providing benefits in the setting of general dental practice.

In clinical practice, a simpler approach such as simultaneous implant placement with guided bone regeneration (GBR) can be adopted for type 1/4 alveolar bone defects, while materials with space-maintaining effects are needed for type 2/4 and type 3/4 defects, and a staged approach

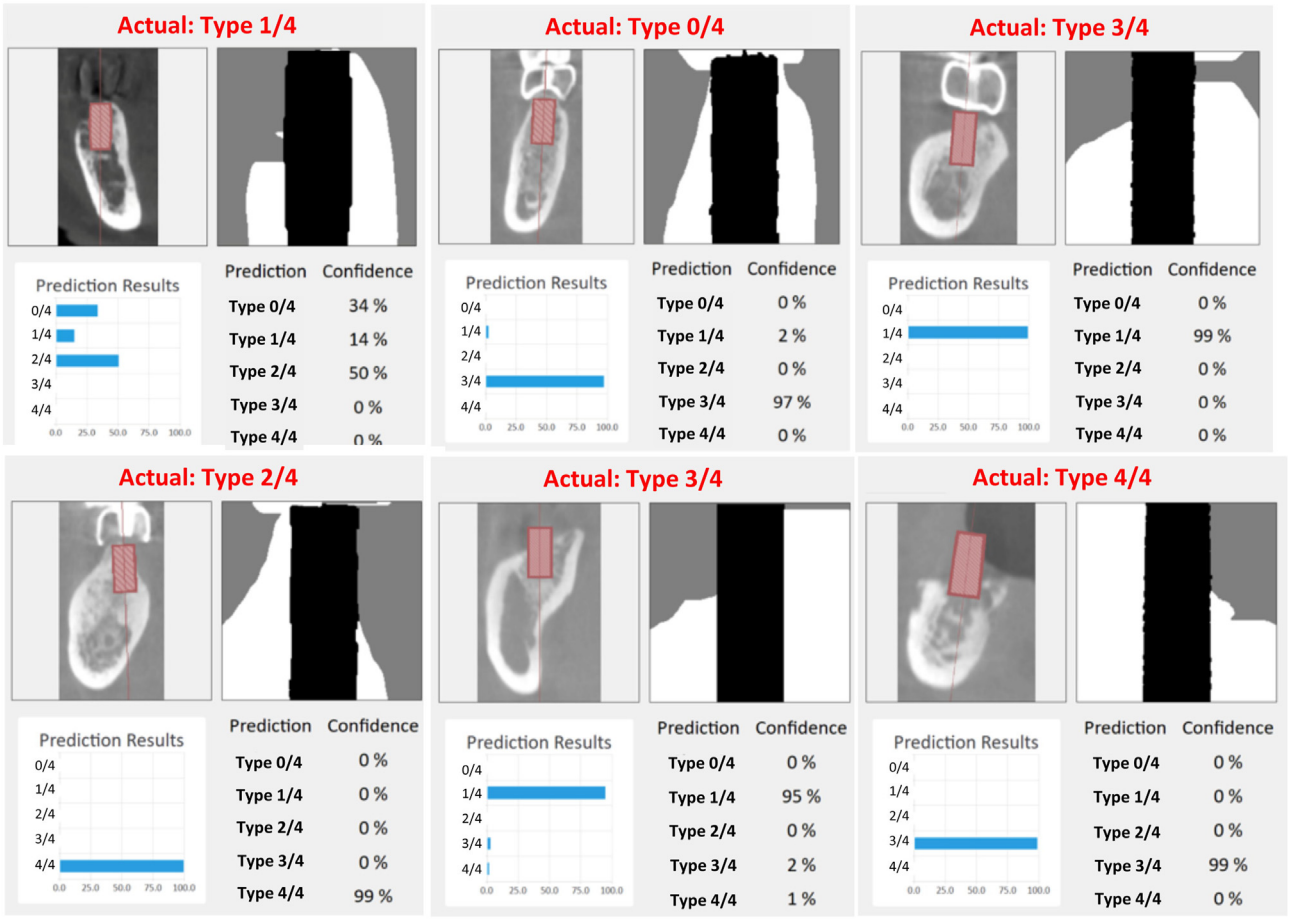

Figure 4 The cases of incorrect classification due to the artifact disturbance in condition C.

may be necessary to reduce the risk of exposing rough implant surfaces. With regard to type 4/4 bone defects, due to the need for rigid materials and the increased difficulty in flap management, an experienced surgeon must design and execute the surgical plan to minimize the postoperative complications. Proper classification of the implant-ridge relationship is crucial for the overall success of the treatment.

To assess the factors influencing the performance of MobileNet for determining the implant-ridge relationship, different sizes of datasets were investigated (conditions A and B), and the results revealed that the model performance was significantly improved when the datasets were larger (Table 2). From these results, the primary source of classification errors seems to stem from preprocessing, particularly the excessive radiopacity caused by the presence of a surgical stent (Figs. 2—4). This issue can be overcome by adopting a fully digital preoperative planning approach without the need for a pre-fabricated surgical stent or a specialized algorithm to remove the surgical stent on the image to eliminate this obstacle. Another issue is related to the presence of air in the oral cavity resulting in image radiolucency. To mitigate this issue, deeper radiolucencies can be filtered out during the K-means stage to minimize this artifact.

Another category was the unidentifiable bone-implant contact; this occurs mainly in cases of thin alveolar bone or a large bone marrow space around the implant (Fig. 2B & 3B). Due to the limitations of CBCT imaging, there is only an approximately 20% probability of detecting a bone thickness of less than 0.5 mm nearby the implant surface. The probability increases to 80% for a bone thickness of greater than 1.2 mm, and nearly all cases are detected when the thickness exceeds 2 mm.[18] Hence, when the bone thickness is less than 1 mm, interpretation errors can easily occur due to imaging artifacts; such errors are difficult to eliminate through increased data or training and may require higher-resolution CBCT imaging devices to effectively address. To overcome the influence of a large bone marrow space, which is typically seen in the mandible,[19] an autofilling algorithm was established for image preprocessing and appeared to reduce the errors in this study. However, due to the discontinuities in cortical bone affecting the K-means clustering process, the filling of the marrow space was still suboptimal in some cases (Fig. 4).

The majority of miscellaneous cases were the borderline cases characterized by a nearly 50% boundary of alveolar bone height according to the definition of the classification.[4] This could be further improved by increasing the volume of data, which would allow the algorithm to accurately identify these borderline cases. Although these cases were statistically considered to be misclassified, they exhibited minimal clinical differences from the perspective of clinicians. Improvements could potentially be achieved

in the future by increasing the resolution of CBCT or exploring other approaches. Furthermore, the difference in the training results between condition B and condition C was minor, suggesting that the autofilling preprocessing algorithm might not be sensitive enough to identify a 'true' bone marrow space. Thus, further improvement of the preprocessing algorithm is still required.

Although implant-ridge relationship identification by MobileNet has reached high accuracy level and could be beneficial to establish reliable clinical diagnosis, this approach still has several concerns. Firstly, the present algorithm relies solely on a single cross-sectional slice from CBCT and might be insufficient to reflect the three-dimensional pattern of ridge defects. The severity of ridge defects might be assessed more accurately when multiple consecutive implants presented, and introducing continuous CBCT slices for AI training will aid in more accurate judgement of the real implant-ridge relationship. Secondly, because the training data was limited to the mandibular posterior region with fully healed ridges, the model's applicability is restricted, and the inclusions of datasets from other regions and unhealed ridges are still required.

In conclusion, we demonstrated that MobileNet architecture was capable of identifying implant-ridge relationship at the clinically applicable level. The results also suggested that AI can assist clinicians in establishing a reliable preoperative diagnosis and treatment plan for dental implants in the setting of general dental practice.

Declaration of competing interest

The authors have no conflicts of interest relevant to this article.

Acknowledgments

The authors acknowledged the support from the Graduate Institute of Clinical Dentistry, National Taiwan University, and the National Science and Technology Council (grant no. 110-2314-B-002-109-MY3).

References

1. Cawood JI, Howell RA. A classification of the edentulous jaws. *Int J Oral Maxillofac Surg* 1988;17:232—6.
2. Seibert J. Reconstruction of deformed, partially edentulous ridges, using full thickness onlay grafts, Part I. Technique and wound healing. *Comp Cont Educ Dent* 1983;4:437—53.
3. Wang HL, Al-Shammari K. HVC ridge deficiency classification: a therapeutically oriented classification. *Int J Periodontics Restor Dent* 2002;22:335—43.
4. Terheyden H. Knochenaugmentationen in der Implantologie. *Dtsch Zahnärztl Z* 2010;65:320—30.
5. Haleem A, Javaid M, Khan IH. Current status and applications of artificial intelligence (AI) in medical field: an overview. *Curr Med Res Pract* 2019;9:231—7.
6. Heidari M, Mirniaharikandehei S, Khuzani AZ, Danala G, Qiu Y, Zheng B. Improving the performance of CNN to predict the likelihood of COVID-19 using chest X-ray images with preprocessing algorithms. *Int J Med Inf* 2020;144:104284.
7. Pal KK, Sudeep K. Preprocessing for image classification by convolutional neural networks. In: *2016 IEEE International Conference on Recent Trends in Electronics, Information & Communication Technology (RTEICT)*; 2016:1778—81.
8. O'Shea K, Nash R. *An Introduction to Convolutional Neural Networks*. 2015. arXiv preprint arXiv:151108458.
9. Li Z, Liu F, Yang W, Peng S, Zhou J. A survey of convolutional neural networks: analysis, applications, and prospects. *IEEE Transact Neural Networks Learn Syst* 2021;33:6999—7019.
10. Du G, Cao X, Liang J, Chen X, Zhan Y. Medical image segmentation based on u-net: a review. *J Imag Sci Technol* 2020;64:020508.
11. Srinivasu PN, SivaSai JG, Ijaz MF, Bhoi AK, Kim W, Kang JJ. Classification of skin disease using deep learning neural networks with MobileNet V2 and LSTM. *Sensors* 2021;21:2852.
12. Velasco J, Pascion C, Alberio JW, et al. *A Smartphone-Based Skin Disease Classification Using Mobilenet Cnn*. 2019. arXiv preprint arXiv:191107929.
13. Jabber B, Lingampalli J, Basha CZ, Krishna A. Detection of covid-19 patients using chest x-ray images with convolution neural network and mobile net. In: *2020 3rd IEEE International Conference on Intelligent Sustainable Systems*. (ICISS), 2020:1032—5.
14. Howard AG, Zhu M, Chen B, et al. *Mobilenets: Efficient Convolutional Neural Networks for Mobile Vision Applications*. 2017. arXiv preprint arXiv:170404861.
15. Mohapatra S, Abhishek N, Bardhan D, Ghosh AA, Mohanty S. Comparison of MobileNet and ResNet CNN architectures in the CNN-based skin cancer classifier model. In: Mohanty SN, Nalinipriya G, Jena OP, Sarkar A, eds. *Machine Learning for Healthcare Applications*. Wiley-Scrivener, 2021:169—86.
16. Association WM. Declaration of Helsinki: ethical principles for medical research involving human subjects. *JAMA* 2000;284:3043—5.
17. Samsuryadi S, Ermatita E. Efficient mobilenet architecture as image recognition on mobile and embedded devices. *Indones J Electr Eng Comput Sci* 2019;22:389—94.
18. González-Martín O, Oteo C, Ortega R, Alandez J, Sanz M, Veltri M. Evaluation of peri-implant buccal bone by computed tomography: an experimental study. *Clin Oral Implants Res* 2016;27:950—5.
19. Oliveira MR, Goncalves A, Gabrielli MAC, de Andrade CR, Vieira EH, Pereira VA. Evaluation of alveolar bone quality: correlation between histomorphometric analysis and Lekholm and Zarb classification. *J Craniofac Surg* 2021;32:2114—8.